Soft Trapping and Manipulation of Cells Using a Disposable Nanoliter Biochamber

Mamadou Diop* and Rod Taylor†
*Department of Physics, The University of Western Ontario, London, Ontario, Canada; and †Institute for Microstructural Sciences, National Research Council of Canada, Ottawa, Ontario, Canada

ABSTRACT Low-power continuous-wave laser radiation is used to form a very stable microbubble at the end of a specially etched and metalized optical fiber probe. We demonstrate that the microbubble, which is firmly attached to the fiber probe, can be used to benignly trap and manipulate living swine sperm cells as well as human embryonic kidney cells. The lifetime of the microbubble has been prolonged and the gaseous environment inside the bubble controlled using micropipette gas injection. The controlled fusion of two microbubbles is demonstrated as a means of transferring microparticles from one bubble to another. These experiments lay the foundation for the use of the microbubble as a mobile, nanoliter-volume disposable biochamber for cellular studies.

INTRODUCTION

Optical tweezers (1–4), tapered micropipettes, and tapered capillary tube probes (5,6) have been used to trap and manipulate microparticles as well as biological material in fluids. The use of laser tweezers is now prolific, however the technique generally requires a sophisticated high-numerical-aperture (NA), short-working-distance optical system and is limited in operation to small fluid depths in low-scattering and low-absorption fluids (7). Micropipettes can be used to trap cells either mechanically or by suction in highly scattering and absorbing fluids. However the hollow sharp tip of a micropipette presents a non-ideal geometry for cell imaging. In addition, tapered micropipettes are generally produced by a pipette puller, and because of that, they have sharp edges that can damage a trapped cell if they are not polished properly (8).

In this article, we introduce an alternative means of trapping and manipulating cells based upon the soft trapping properties of a microbubble formed at the end of a fiber probe. In 2003, Taylor and Hnatovsky showed that a hollow-tip version of a near-field scanning optical microscopy (NSOM) fiber probe that produced an annular light beam could trap a glass microbead in 3-D in water (9). They observed that when the continuous-wave (CW) laser light coupled into the fiber was increased to slightly higher than 10 mW and incident on a partially metalized probe tip, it was possible to create a very stable microbubble centered on the microtip. Once the microbubble was created, the laser power could be shut off and the bubble decayed slowly away. The process was highly reproducible and could be repeated over and over again. In a later publication (10), they demonstrated that a stable spherically symmetrical microbubble could be produced in many liquids at the tip of this modified NSOM probe and used to trap, manipulate, and mix micron-sized particles on the bubble surface. We now lay the foundation for practical biological applications of this microbubble. The ease in controlling the microbubble's position by manipulating the fiber probe in 3-D has allowed us to benignly trap, manipulate, and release vigorously moving swine sperm cells. Soft trapping of human embryonic kidney cells (HEK-293) is also demonstrated.

The concept of using the microbubble as a biochamber is also proposed and validated in this article. The microbubble provides a new (liquid/gas) trapping surface compared to the standard liquid/glass interface of a glass microscope slide or a glass micropipette covered with a liquid. Since the movement of cells and cell adherence can be affected by their physical interaction at the substrate surface (11), quite different behavior may be obtained on the bubble surface. Indeed the new surface more closely resembles that of a standard liquid/air interface but has a spherical geometry of small size and can be moved anywhere underneath the liquid surface. It might be particularly useful for the rapid formation of bacterial films with nutrients supplied to the film on the liquid side of the bubble and a gas of the experimenters' choice (e.g., O_2) supplied on the other side of the bubble.

We show that dissolved gases such as air play a dominant role in the bubble stability and establish that the bubble lifetime is determined by gaseous diffusion through the gas/liquid interface and not by vapor condensation, in accordance with Epstein and Plesset's theory (12). For practical applications we also demonstrate that the lifetime of the bubble can be increased even further from the lifetimes mentioned in Taylor and Hnatovsky (10). To this end, we show that tapered micropipettes can be used to inject different gases inside the microbubble to sustain it against collapse and create a controlled environment inside the bubble. Finally, the possibility of fusing two microbubbles together, in a controlled manner, and the use of this method to transfer microparticles from one bubble to another is demonstrated.

Submitted October 5, 2005, and accepted for publication February 6, 2006.
Address reprint requests to Rod Taylor, E-mail: rod.taylor@nrc-cnrc.gc.ca.

0006-3495/06/05/3813/10 $2.00
doi: 10.1529/biophysj.105.075614

THEORY

The creation phase of our microbubble lasts for only a few seconds. Once the bubble is formed, the CW laser beam is shut-off. Due to the small dimensions of the metalized fiber probe ($\leq$125 μm), the temperature rapidly drops to ambient temperature on a similar timescale of a few seconds (refer to Appendix). Therefore, bubble decay, which takes place over many minutes to hours, can be well separated from the formation process. We use the theoretical treatment for bubble collapse established by Epstein and Plesset (12), based upon diffusion of trapped gases through the bubble surface, to describe our bubble dynamics. We make the assumption that condensation of water vapor trapped in the bubble plays a minor role in bubble decay and can be ignored in this theoretical model. In our experiments, since the bubble is firmly attached to the fiber and immobile, we can neglect buoyancy forces and any movement of the bubble through the liquid.

Starting with the diffusion equation

$$\partial c/\partial t = \kappa \Delta c, \tag{1}$$

it has been established (12) that when the liquid is undersaturated with gas, the bubble radius obeys the following differential equation:

$$dR/dt = -\alpha(1/R + 1/(\pi\kappa t)^{1/2}). \tag{2}$$

The effect of the surface tension on the bubble decay is neglected here. A more complete theoretical treatment, taking into account the surface tension, showed that this assumption is justified (12).

When enough time has elapsed for significant diffusion to take place, the solution of the previous equation is

$$\varepsilon^2 = 1 - x^2, \tag{3}$$

with

$$\varepsilon = R/R_0, \tag{4}$$

$$x^2 = (2\alpha/R_0^2)t, \tag{5}$$

$$\alpha = \kappa(c_s - c_i)/\rho. \tag{6}$$

R is the bubble radius at time t, R_0 is the initial bubble radius, κ is the coefficient of diffusivity of the gas in the liquid, c_i and c_s are respectively the initial and saturated dissolved gas concentrations in the solution, and ρ is the gas density inside the bubble.

Substituting these values in Eq. 3 yields

$$(R/R_0)^2 = 1 - (2\kappa(c_s - c_i)/\rho R_0^2)t. \tag{7}$$

Eq. 7 can be expressed in terms of the bubble diameter:

$$(D/D_0)^2 = 1 - t/\tau_0, \tag{8}$$

with

$$\tau_0 = \rho D_0^2/8\kappa(c_s - c_i), \tag{9}$$

τ_0 being the bubble lifetime expressed in terms of the properties of the dissolved gas in the liquid.

The theory predicts that the bubble lifetime depends quadratically on the bubble's maximum diameter resulting in enhanced lifetimes for large bubbles. Eq. 9 also predicts that long bubble lifetimes will occur for bubbles containing a high-density gas that has a low diffusivity into the liquid. Long lifetimes will also be achieved when the initial and saturated gas concentrations are close in value.

In the case of a water solution oversaturated locally with air (i.e., the local $c_i > c_s$, where the c_s value is appropriate for the bulk liquid), the resolution of Eq. 1 predicts a growth of the bubble governed by an equation similar to Eq. 8 but with a positive slope:

$$(D/D_0)^2 = 1 + t/\tau_0 \tag{10}$$

and now with

$$\tau_0 = \rho D_0^2/8\kappa(c_i - c_s). \tag{11}$$

MATERIALS AND METHODS

Generation of a stable microbubble

The microbubbles were generated using an experimental setup similar to the one described in previous articles on microbubbles by Taylor and Hnatovsky (10,13). The light source was a polarized CW laser (Lightwave Electronics, Mountain View, CA) emitting at 1.32 μm. The laser radiation was passed through a mechanical shutter (Newport Corp., Irvine, CA) with a digital controller (Newport Corp.). A half-wave plate was used to rotate the polarization and combined with a polarizer to act as a variable attenuator of the laser power coupled into the fiber. After the polarizer, the beam was passed through a nonpolarizing beam-splitter and coupled into the core of an ~0.5-m-long single-mode optical fiber (Fibercore Ltd., Southampton, England) using a coupling microscope objective with an NA of 0.32. Laser powers in the range 10–30 mW were typically coupled into the fiber. The output end of the fiber which had a specially designed selectively chemically etched conical tip with a hollow reservoir (9,10,13) was immersed in a droplet of the medium a few mm thick, where the microbubble was to be generated. The fiber was placed in a holder mounted on a stage that could be tilted and moved in 3-D with micrometric control. The holder could also be rotated, enabling the rotation of the microbubble. An overhead microscope (Nikon, Tokyo, Japan) with different microscope objectives together with a digital camera (Opti-Tech Scientific, Scarborough, ON) or a SensiCam high-performance monochrome charge-coupled device (CCD) camera (The Cooke Corp., Auburn Hills, MI) was used to image the fiber-tip region.

A part of the light traveling down the fiber was retroreflected from the metalized (Pt) tip and returned through the coupling microscope objective to be directed by the beam-splitter to a powermeter (Newport Corp.) for detection. The back-reflected signal at the detector (Newport Corp.), which consisted of a small depolarized component due to the polarizing scrambling nature of the fiber, was optimized to ensure that the laser light was efficiently coupled into the small-diameter core and then directed all the way to the fiber tip.

Microbubble decay measurements

For the experiments designed to explore the role of air in microbubble decay, room-temperature fresh tap water, partially degassed tap water, partially degassed tap water with air injected inside, and distilled and deionized water were used. The degassing was done by boiling two liters of tap water for 2 h in an Erlenmeyer flask. To improve the degassing, the water was stirred during the entire boiling process using a bar magnet. A volume of 5 mL of the boiled water was taken from the center of the flask using a syringe, and cooled (in the

syringe) to 19°C by passing it under the flow of cool tap water. Thereafter, a Millex-GV syringe-driven filter unit with a pore diameter of 0.22 μm (Millipore Corp., Carrigtwohill, Ireland) was mounted at the syringe output to filter the cooled boiled tap water. The filtering permitted the removal of by-products from the boiling procedure that could eventually accumulate on the fiber probe tip and make the probe rapidly unusable. The cooling and the filtering process took ~2 min. After that, the filtered bead of water was placed on the glass microscope slide and the microbubble immediately generated. The boiled tap water with air blown inside was obtained by vigorously blowing air for 15 min in already-boiled tap water, prepared as described previously, using air blasts from a compressed air cylinder.

Trapping of cells

In the sperm trapping and releasing experiment, the sperm used were capacitated swine sperm (14) diluted in HEPES-buffered Krebs Ringers Bicarbonate (KRB-HEPES). The composition of the KRB-HEPES solution was 119.4 mM NaCl, 4.8 mM KCl, 1.7 mM $CaCl_2$, 1.2 mM KH_2PO_4, 1.2 mM $MgSO_4$, 25 mM sodium lactate, 1 mM sodium pyruvate, 5.6 mM glucose, 28 μM phenol red, 4 mM $NaHCO_3$, and 21 mM Hepes, pH 7.4. Human embryonic kidney cells were also trapped and imaged. The HEK-293 cells were frozen in dimethylsulfoxide at −80°C and stored until use. Once it was taken out of the refrigerator, we placed the vial containing the concentrated cell solution in a container with ice cubes to let the cells slowly warm up to 0°C. After that, a drop of the concentrated HEK-293 solution was deposited into a new vial and diluted with a phosphate buffer (137 mM NaCl, 1.5 mM KH_2PO_4, 8.1 mM Na_2HPO_4, and 2.7 mM KCl, pH 7.3) to the desired concentration. The diluted HEK-293 cell solution was gently stirred up before use to get a homogeneous solution. Thereafter, a drop of the diluted cell solution was added to a bead of water (water was used for demonstrating the technique only; the appropriate biological medium has to be used for trapping living cells) in which the microbubble was already generated. Under the force of gravity, the cells fell to the glass slide. Using a high-NA (0.75) microscope objective, we imaged the cells on the glass slide as the microbubble was brought into contact with the cells using the micromanipulators. Once the microbubble was in contact with the cells, there were two options for trapping the cells. One was by moving the microbubble via the micromanipulators. The second method was to move the fluid around the microbubble by moving the glass slide. With this last method, one had to be careful to avoid dislodging the microbubble from the fiber probe. Once the cells stuck to the microbubble surface, the microbubble was raised from the glass slide using the micromanipulators.

Micropipettes and fusion of microbubbles

The micropipettes used to penetrate the bubbles and the cells were fabricated using Borosilicate capillaries (World Precision Instrument, Sarasota, Florida) of 1.5-mm outer diameter. The capillaries were pulled with a micropipette puller (Sutter Instruments, Novato, CA), down to a tip with a diameter of a few microns or less(~0.5 μm). The micropipettes were placed in a home-made holder and mounted on a stage to position the tips at the desired location with micrometric control. The insertion of the micropipette into the cell was done by finely moving it using the micromanipulators. For the gas- and particle-injection experiments, the micropipettes were mounted on a holder attached to a microinjector (Eppendorf, Westbury, NY). The microinjector was connected to a cylinder of a compressed industrial-grade gas (He, from Air Liquid Canada, Ottawa, ON, or N_2, from BOC Gases Division of Canada, Gloucester, ON), using a 6-m-long flexible tube.

We used 2-μ-diameter (uniform glass microspheres; Structure Probe, West Chester, PA) and 100-nm-diameter fluorescent particles (TransFluoSpheres, carboxylate-modified microspheres; Molecular Probes, Eugene, OR) absorbing at 488 nm and emitting at 560 nm. An argon-ion laser (Omnichrome, Chino, CA) emitting at 488 nm was used to excite the fluorescence of these submicron particles.

Two methods were used to fuse microbubbles in a controlled manner. In the first one, a microbubble was generated at the tip of the fiber into which the laser radiation was coupled (''active'' fiber). This bubble was then transferred to a ''neutral'' fiber (a fiber that was only stripped and cleaved, and without any metal coating or laser light coupled inside). After that, a second microbubble was generated at the tip of the ''active'' fiber and the two microbubbles were pushed one against the other to fuse. The second technique consisted of bringing the two microbubbles into contact and directing the CW laser radiation into the ''active'' fiber, to a power level equal to or higher than the bubble-generation threshold power (≈12 mW in the tap water), for a short duration of 10 ms.

Note that all the experiments described in this article were done at atmospheric pressure and ambient temperature.

RESULTS

Control of the microbubble size and lifetime

The microbubble's maximum diameter was set by choosing the laser power and the shutter opening time. Fig. 1 shows the variation of the bubble's maximum diameter versus the shutter opening time for three different CW laser powers (19.4, 24.2, and 28.7 mW). The microbubble diameters were obtained with an accuracy of ≈2% by direct measurement of the CCD images. The maximum microbubble size that can be obtained is mainly limited by the mechanical stability of the microbubble at the fiber probe tip when the bubble diameter becomes much larger than the fiber diameter. The fiber probe used in these experiments (initial cladding diameter, 125 μm) can handle a microbubble as large as 450 μm without it being dislodged.

To investigate the role of air trapped in water on the microbubble decay, we measured the diameter versus time of microbubbles generated in boiled tap water and boiled tap water with air blown inside. Fig. 2 shows that for the same starting diameter (D_0 = 95 μm), the bubble generated in boiled tap water decayed faster (3.7 min) than the one produced in boiled tap water with air blown inside (10.5 min). In Fig. 3, we show a comparison between the experimental data from Fig. 2 and the theoretical predictions for microbubble decay using Eq. 8 from the Epstein-Plesset

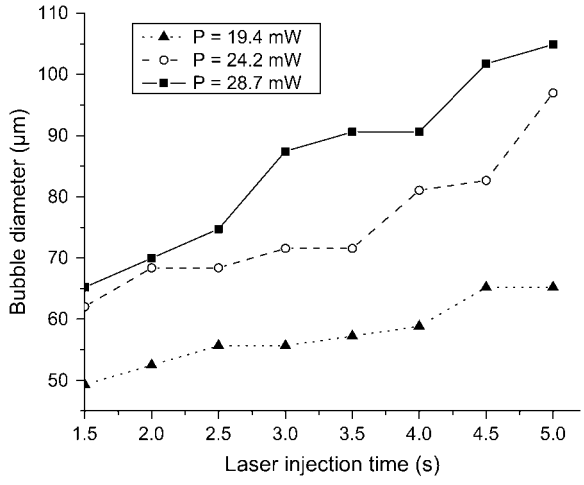

FIGURE 1 Control of the microbubble's maximum diameter by increasing the shuttered laser injection time for three different CW laser powers.

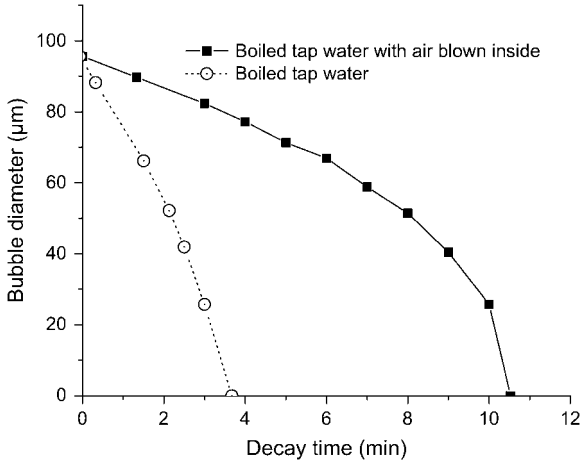

FIGURE 2 Decay of the microbubble diameter as a function of time in boiled tap water and boiled tap water with air blown inside. The lines are used for guiding the eyes only.

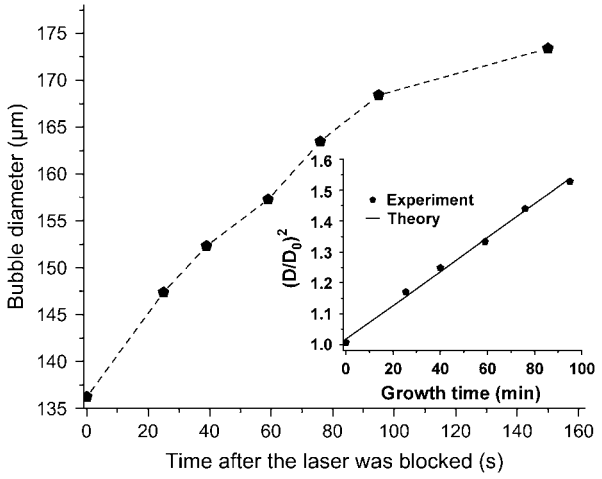

FIGURE 4 Growth of the diameter of a microbubble generated in fresh tap water after the laser beam was blocked. (*Inset*) Experimental data points and simulation (*solid line*) using Eq. 10.

theory. The intercepts of the simulation curves (Fig. 3) with the decay-time axis predicts a lifetime of 3.1 min for the microbubble generated in boiled-only tap water and 11 min for the one in boiled tap water with air blown inside.

We also noted that the diameter of a microbubble generated in fresh tap water continued to grow after the laser beam was blocked despite the fact that the probe tip cools off very rapidly (see Appendix and Taylor and Hnatovsky (10)), implying that the growth is not due to any heating of the microbubble after the laser radiation has been blocked. This behavior was not observed in boiled tap water. In Fig. 4, the microbubble diameter increased from ~135 to 175 μm, 150 s after the laser beam was blocked. At longer times the bubble expansion tended toward a limiting diameter. This expansion was observed in fresh tap water for microbubbles with diameters as small as 40 μm. This was the minimum bubble diameter that we could perform the experiment with sufficient accuracy. The inset of Fig. 4 shows the experimental data points, excluding the last data point, which is in a growth saturation regime, and the prediction from Epstein and Plesset's theory (Eq. 10) based upon a locally oversaturated air-water solution just outside the bubble.

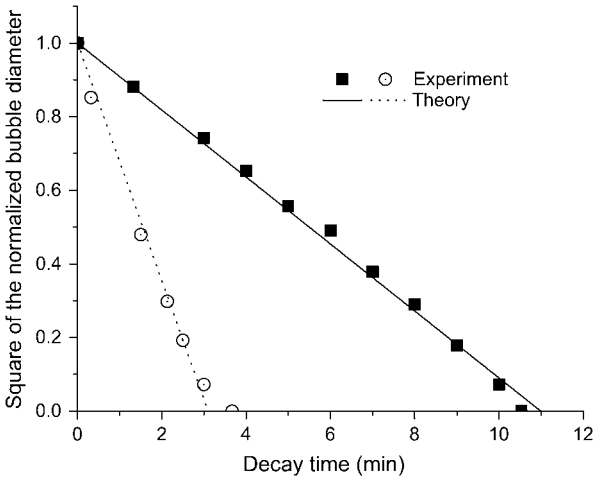

FIGURE 3 Experimental data points taken from Fig. 2 and simulation (*lines*) using Eq. 8.

Microbubble trapping of cells

In this section, we show that the microbubble can be used to trap, manipulate, and image a single vigorously moving swine sperm. Fig. 5 shows images taken from a movie showing a sperm trapped on the surface of a microbubble generated in KRB-HEPES solution. The flat body of the sperm adhered to the bubble at a fixed location (the sperm tail was free to move, allowing the body of the sperm to rotate about a fixed position) for approximately half an hour until the microbubble collapsed to a small size ($D \cong 20$ μm), releasing the sperm, which swam away. The sperm was still

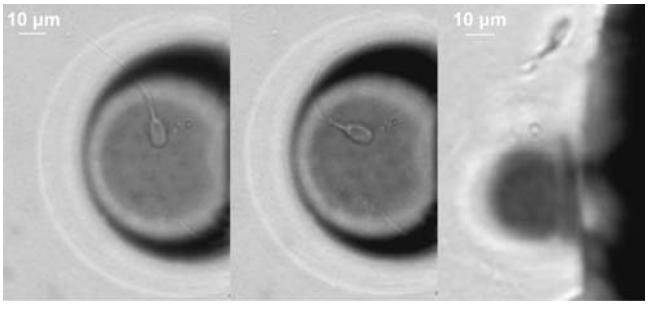

FIGURE 5 Trapping (first two frames, taken at different times) over a half-hour period and releasing (last frame) of a single highly motile swine sperm.

alive and vigorous after it had been released. The time at which the sperm was released was related to the size of the microbubble. As the bubble diameter decayed, the rate of decay (Eq. 2) increased and the bubble collapse accelerated. This caused changes in the convective fluid flow around the bubble, which dislodged the sperm.

One or multiple HEK-293 cells were selectively trapped on the microbubble surface. The number of cells trapped depends on the cell concentration around the microbubble. By carefully setting the concentration of the diluted solution of cells we were able to trap a single cell (Fig. 6, *a* and *b*). After they have were trapped on the microbubble, the cells initially moved around the microbubble surface due to fluid flow but became immobile after a few minutes (between 5 and 15 min, depending on the degree of agitation of the fluid). After approximately 2 h, they adhered very strongly to the microbubble surface as shown in Fig. 6 *c*, although by this time the cells were surely dead.

We were able to change the position of the cell on the microbubble surface by moving the microbubble or the fluid via a displacement of the glass slide and by rotation of the fiber holder. A single cell trapped on the microbubble surface could be moved to the desired position to be imaged and penetrated by a probe, as shown in Fig. 6 *d*. We successfully penetrated the cell and into the microbubble without damaging the fragile highly tapered micropipette. Once the micropipette was inserted into the cell, we were able to use it to move the cell around the microbubble surface or to inject dye inside the cell. We have also used the microbubble technique to remove HEK-293 cells that appeared stuck to the glass slide, without using complicated and expensive equipment such as pulsed lasers (15).

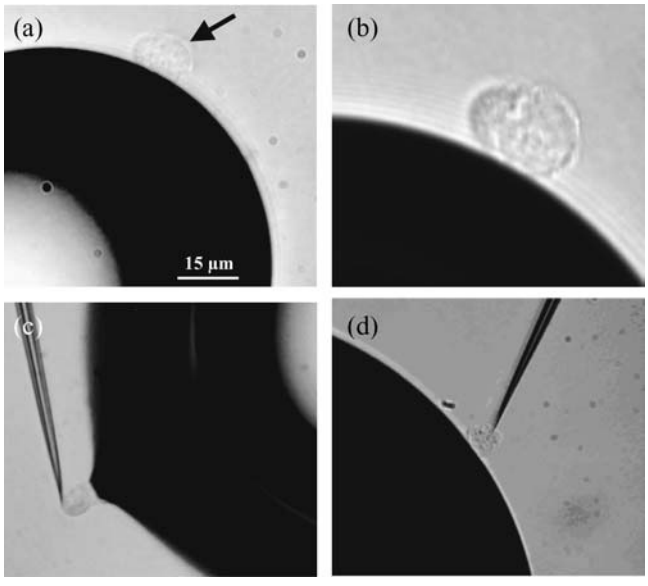

FIGURE 6 (*a*) A HEK-293 cell (*arrow*) benignly trapped on a microbubble. The higher magnification (*b*) shows details of the cell. (*c*) Micropipette-controlled distortion of both a HEK-293 cell and the microbubble surface, demonstrating substantial cell adherence and the deformability of the microbubble. (*d*) A HEK-293 cell trapped on the microbubble surface and penetrated with a tapered micropipette.

Controlled micropipette injection of gas into the microbubble

We have routinely demonstrated that a microbubble attached to our modified NSOM fiber probe can be penetrated with tapered micropipette probes (tip diameters 0.5–3 μm) without altering the bubble shape. During the penetration, the microbubble did try to move away from the micropipette but usually remained firmly attached to the fiber end face. When the penetration was completed, the microbubble regained its spherical shape. Table 1 indicates that when a micropipette is inserted inside the bubble (while the other end of the micropipette is at atmospheric pressure), there is a decrease of only 5–10% in the microbubble lifetime with respect to the lifetime of another bubble of the same size but without a micropipette inside. The penetration was done at very different angles (from 0 to 90° with respect to the fiber axis) and multiple penetrations had no apparent impact on the bubble symmetry.

Using a microinjector and a tapered micropipette, we succeeded in injecting N_2 and He gases inside the microbubble in a controlled manner. The data in Table 2 demonstrate the accurate control of the microbubble size by injecting N_2 gas through the micropipette. We were able to increase the microbubble diameter in increments as small as 1 μm and in volume steps as small as tenths of nanoliters. To control the environment inside the microbubble, the initial gases and vapor are purged and the desired gases injected inside the bubble. This is done by simply injecting the gases and waiting until the bubble decays to a small diameter, then injecting the gases again and repeating the process until the concentration of the desired gases is reached. We have realized this by injecting He gas (see Table 3), but this can also be done using many other gases. The data in Table 3, for helium injection, also show that the bubble can be sustained for >5 h (319 min) using this technique.

The micropipette, which can be moved to any position inside the bubble, has also been used to inject micro- or nanoparticles into the bubble. We observed that the small-diameter (100-nm) dye particles, initially injected into the interior of the bubble, rapidly (within seconds) moved to

TABLE 1 Difference in microbubble lifetime with and without a micropipette inside

Initial diameter (μm)	Bubble lifetime (min) without the micropipette	Bubble lifetime (min) with the micropipette	Difference in bubble lifetime (%)
85	12.9	12.1	6.2
99	14.5	13	10.3
107	20.7	19.6	5.3

TABLE 2 Demonstration of accurate control of the microbubble volume by means of micropipette injection of N_2 gas

Initial bubble diameter (μm)	Initial bubble volume (10^6 μm^3)	Final bubble diameter (μm)	Final bubble volume (10^6 μm^3)	Volume increase (nL)
65	1.1	66	1.2	0.1
58	0.8	65	1.1	0.3
80	2.1	100	4.2	2.1
115	6.4	208	37.7	31.3

the bubble surface as shown in Fig. 7. The maximum size of the particles that can be injected is limited by the micropipette tip aperture to a few microns. If the particles are too heavy, they will fall under gravity but still stay on the bubble surface.

Controlled fusion of two microbubbles

The upper panel of Fig. 8 shows the fusion of two microbubbles by pushing one against the other. With this method, we observed that some of the time one of the bubbles was dislodged from the fiber and the process had to be restarted. In the lower panel of Fig. 8, we demonstrate the fusion of two microbubbles by initiating a burst of laser radiation at a power level of ~12.5 mW for only 10 ms. This technique was much more reliable and we have never dislodged a bubble with this method. If the power was less than the bubble generation threshold power (≈12 mW for fresh tap water), the bubble on the ''active'' fiber grew in size but there was no fusion even if the laser radiation was coupled into the fiber for a long time. With this technique, the fusion process occurs in ≤1 ms, as determined by the time between two consecutive frames on the SensiCam QE CCD camera. During the fusion of two microbubbles, generally the smaller bubble detached and fused into the bigger one but this could be reversed if the smaller bubble was on the ''active'' fiber (Fig. 8, *lower panel*).

The volume of the final bubble was within 0.8% of being equal to the sum of the two initial bubble volumes (see Table 4). The final bubble could be fused with another one, and the process could be repeated over and over again as long as the final bubble could be handled by the fiber.

TABLE 3 Sustaining a microbubble by means of multiple micropipette injections of helium

Initial diameter (μm)	Final diameter (μm)	Diminution of the diameter (μm)	Decay time (min)
148	94	54	13
206	115	91	50
146	118	28	29
161	111	50	56
154	119	35	30
144	114	30	18
217	91	126	123
		Cumulative sustaining time	319

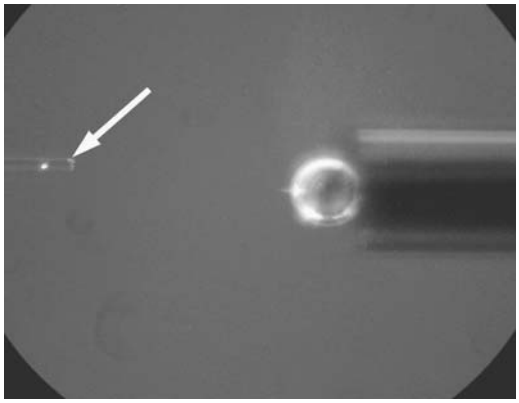

FIGURE 7 Fluorescent submicron particles injected inside a microbubble via a micropipette (*arrow*) moved within seconds to the microbubble surface. Notice that the dye fluorescence is pronounced on the surface of the microbubble. The diameter of the fiber probe holding the bubble was 118 μm.

DISCUSSION

Microbubble growth and decay dynamics

The microbubble is initiated by highly localized heating and spontaneous boiling of the liquid from the last few microns of the metalized tapered tip, which corresponds to the position of the maximum light absorption. The sudden formation of the bubble creates a local high pressure of vapor and trapped gases, which initiates the microbubble growth process. The bubble rapidly expands symmetrically about the tip to diameters that depend on the laser power and the duration of the coupling of the laser radiation into the fiber (Fig. 1).

The microbubble generated in the boiled tap water with air blown inside has a longer lifetime than the bubble with the

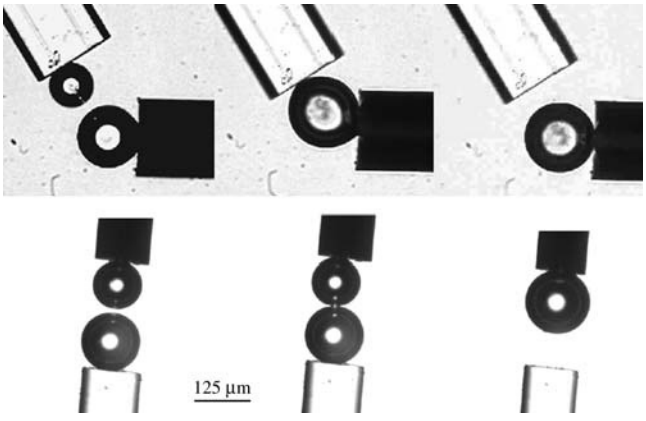

FIGURE 8 (*Upper*) Transfer of 2-μglass particles (shown in the center of the top bubble) from the surface of one microbubble to another by fusing one bubble into the other. (*Lower*) Controlled fusion of two microbubbles by directing a shuttered burst of laser radiation into the ''active'' fiber (*top*) that held the smaller bubble. The laser power was 12.5 mW and the burst duration was 10 ms.

TABLE 4 Controlled fusion of two microbubbles

	Example 1	Example 2
Diameter of bubble A (μm)	111	88
Diameter of bubble B (μm)	147	169
Diameter of the final bubble (μm)	166	177
Volume of bubble A (10^6 μm^3)	5.7	2.8
Volume of bubble B (10^6 μm^3)	13.3	20.2
Volume of bubble A + volume of bubble B (10^6 μm^3)	19.0	23.0
Volume of the final bubble (10^6 μm^3)	19.1	23.2
Difference in volume (%)	0.5	0.8

same initial diameter created in the degassed boiled tap water (Fig. 2). As the only difference between the two types of water is their air content, the difference in lifetime is therefore related to the difference in trapped air concentration. Indeed, it is well known that the solubility of air in water decreases when the temperature increases. This fact combined with the degassing due to boiling and stirring notably reduced the concentration of air in the water after 2 h of boiling. Therefore, the initial concentration (c_i) of the dissolved gas in the boiled tap water with air blown inside is greater than in the boiled-only tap water, and Eq. 9 predicts that a microbubble generated in the first medium has a longer lifetime than a bubble, with the same initial diameter and at the same temperature, created in the degassed tap water. In Fig. 3, there is a small difference between the theoretical predictions (obtained using Eq. 8) for the lifetimes based upon the extrapolation of the simulation curves to $D = 0$ μm and the experimental data points. The difference is due to the difficulty of precisely measuring the last experimental data point when the microbubble collapse accelerates to rapidly approach zero size. If one excludes the last experimental data point for this reason, there is very good agreement between the experimental data and the simulation in Fig. 3.

These results support the validity of the theoretical model and strongly suggest that the bubble decay is governed by air diffusion through the microbubble surface rather than by condensation of the vapor at the microbubble wall. One consequence of microbubble decay that is dominated by gaseous diffusion is that it should be possible to increase the lifetime of bubbles in different liquids by saturating them with air or with other gases.

A qualitative explanation for the bubble growth obtained in Fig. 4 (after laser shut-off) and subsequent decay dynamics (Fig. 2) proceeds as follows. In a previous work, (10), the authors showed that convective fluid flow by means of the Marangoni effect can drive micron-sized glass particles toward the microbubble during its creation phase. They also demonstrated that blocking the laser beam immediately stopped the convective flow. If we assume that air is trapped in water as very tiny air pockets, it can be argued that these air pockets are carried to the microbubble in a way similar to that of the glass microparticles. The flow of air toward the microbubble can lead to saturation of the local air content in the liquid surrounding the bubble. When the laser beam is blocked, the liquid very close to the microbubble is almost saturated with air and the bubble keeps on growing due to diffusion of air through the interface to the interior of the bubble. There is also diffusion of air from the saturated zone (close to the microbubble) to the bulk of the surrounding liquid due to a concentration gradient. At a certain time, the concentration inside the microbubble and in its vicinity equilibrates and the microbubble growth stops. As the concentration in the domain close to the microbubble is still higher than in the bulk solution, the diffusion of air from that zone to the liquid continues and the concentration in the vicinity of the bubble drops. This causes a concentration gradient between the interior of the microbubble and its vicinity that, in turn, causes the diffusion of air from within the microbubble to the local air-unsaturated liquid surrounding it. This explains why the microbubble grows after the laser radiation is blocked (Fig. 4), but ultimately decays after it reaches its maximum size (Fig. 2). The excellent agreement between the Epstein-Plesset theory for an over-saturated air solution (Eq. 10) and the experimental bubble growth shown in Fig. 4 provides further support that the diffusion-based theory accurately predicts the bubble dynamics.

Microbubble for trapping biological material

One can think of the microbubble attached to the end of an optical fiber probe as a kind of optical tweezer. The laser radiation coupled into the fiber probe does not trap biological material directly (i.e., in a noncontact way using only light for trapping); however, it does create the trapping structure, i.e., the microbubble. The bubble diameter is generally quite large compared to typical focal-spot sizes of $\sim$1 μm used in laser-tweezer experiments, and therefore the precision of trapping, manipulating, and releasing an object is poorer (estimated to be $\sim$5 μm). Also, the optical-tweezer trapping action can occur within biological material, for example, to manipulate individual cellular components. This is not possible with microbubble trapping. Nonetheless, the microbubble can accomplish many of the tasks that optical tweezers perform, including damage-free trapping of biological material, such as cells. However unlike optical-tweezer trapping, microbubble trapping can be performed in highly turbid or absorbing fluids and at great depths (millimeters to centimeters). Microbubble trapping does not impose any restriction on the optical absorption properties of the biological object to be trapped. This is in complete contrast to optical tweezers, where too much absorption of the laser light by the biological object can lead to thermal damage. However, it should be noted that it is prudent to create the microbubble away from the object to be trapped to avoid any chance of thermal damage. Finally the microbubble with an attached biological specimen can more easily

and rapidly (mm/s) be maneuvered in 3-D than material trapped by optical tweezers. Multiple traps are possible with additional fiber probes or by means of creating and detaching a microbubble onto some substrate (as in Fig. 8), then creating another bubble, etc.

At this stage, it is not clear how the microbubble actually traps cells and we need to better understand the role of surfactants associated with the organic material or amphipathic substances produced by the living organisms present in the solution in altering the surface tension and adhesion properties at the microbubble surface. During the HEK-293 cell trapping experiments, we observed a substantial increase in the bubble lifetime (>5 h for a microbubble of ~150 μm in diameter) compared to that observed in water (e.g., 58 min for a microbubble with an initial diameter of 190 μm). The extra-long lifetime may be a consequence of surfactant that can stabilize the bubble, possibly by interfering with the gaseous diffusion through the microbubble wall.

The microbubble trapping technique might be very useful for in vitro fertilization (IVF) studies. The microbubble, which is attached to the fiber probe, can be suitably placed above a pool of sperm to select and trap a single vigorous sperm, as demonstrated in this study. Once trapped, the sperm can be manipulated and brought to the focus of a high-resolution imaging system to obtain a detailed morphology of the sperm before the IVF process. At present, identification of sperm based on morphology is limited to gross identification of whether the sperm is functional, bent, or nonfunctional. This simple technique could provide researchers with a better screening procedure for IVF. The technique could also be used to deliver and deposit the selected sperm to a desired site on the oocyte. The sperm selection process can be repeated many times by simply creating a new microbubble at the end of the fiber probe.

Microbubble as a disposable miniature biochamber

One can also think of the stable microbubble as a mobile disposable biochamber. The liquid/gas interface on the microbubble provides an essentially impenetrable boundary to the movement of liquid flow and particle penetration into the bubble. In this article, we have shown that this boundary can be used to trap cells and that it is possible to surround the cells with either nanoparticles (Fig. 7) or micron-sized beads (Fig. 8), which could lead to a method for slow-release drug/toxin delivery to the exterior of a cell. Of course, the drugs (toxins) would then have to pass through the cell-membrane barrier. We have also shown that it is possible to change the composition of the gas in the interior of the bubble. Since there appears to be strong adhesion of both the sperm cells (Fig. 5) and the HEK-293 cells (Fig. 6) to the bubble surface, that part of the cell surface which is attached to the bubble should be exposed to the gas environment inside the bubble via gaseous diffusion.

During the bubble fusion using the ''pushing technique,'' the mechanical force applied by the pushing completely expelled the liquid between the two microbubbles, allowing disruption of the blended interface of the bubbles, which resulted in their fusion. In the second method, the fusion is initiated by the pressure pulse created by the laser burst. The short duration of the laser burst ensures that there is very little heating of the microtip and even less heating of the microbubble surface. This is very important in avoiding thermal damage of a cell trapped on the bubble. The bubble fusion technique can be used for transporting particles from one bubble to another (Fig. 8) or possibly delivering drugs to a single biological specimen such as a cell trapped on the microbubble surface.

The results presented in this article demonstrate the feasibility of using other tapered probes such as high-optical-resolution NSOM fiber probes (16,17) and patch-clamp probes (18) for single-cell probing. The microbubble might also provide an alternative surface interface (liquid/gas) for the study of a cell's electrical activity. For example, microelectrodes could safely penetrate the microbubble to sit on either side of the cell for voltammetry measurements (19), without any dramatic disruption of the microbubble.

CONCLUSIONS

The excellent agreement between our experiments and the Epstein and Plesset's theory demonstrates that CW laser-induced microbubble growth and decay dynamics are governed by gaseous diffusion through the bubble surface rather than by vapor condensation. This makes it possible to produce long-lifetime microbubbles in a wide range of liquids that have reasonable air (gas) content. Injection of gases into the microbubbles can further increase the lifetime of the microbubble to permit trapping, imaging, and release of biological specimens such as the sperm sample used in this study. The very stable microbubble may also permit the study of living cells and their response to mechanical, electrical, chemical, and biological stimuli over a prolonged period of time.

The ability to alter the interior environment of the microbubble by the injection of gases and control of the bubble temperature using the microtip heater creates a microbiochamber where small quantities of biological material can be studied. The novel aspect of a highly curved and controllable microbubble surface attached to the end of a fiber probe, which can easily be manipulated in 3-D within the bulk fluid, should make it very interesting for the study of cell adhesion, cell-cell interactions, and cell growth compared to studies performed on conventional glass slides.

As a final remark, we emphasize that the apparatus for forming the microbubble is very straightforward to use. The most difficult part of a microbubble experiment is efficiently coupling the laser light into the small core of the fiber probe. The use of commercially available lasers with electronic control of the laser power and direct coupling of the fiber to the

laser output window will make the apparatus simple to use by experimenters who are not experts in lasers and optics.

APPENDIX

A more complete analysis than that given by the Epstein and Plesset's theory (12) used herein should include a combination of the Rayleigh-Plesset equation (20) and the diffusion equation. Such a theoretical treatment is beyond the scope of this article.

However, when the bubble reaches its maximum size (e.g., 175 μm for the microbubble of Fig. 4), just before it begins to collapse, the pressure balance over the bubble's surface gives

$$P_B = P_L + 4\sigma/D. \quad (12)$$

P_B is the entire pressure inside the bubble, P_L is the pressure inside the liquid far away from the bubble, $4\sigma/D$ is the pressure due to the surface tension, σ is the surface tension of the liquid, and D is the microbubble diameters.

Eq. 12 can be used to calculate the pressure inside the microbubble provided the values of the pressure inside the liquid (water in our case), the microbubble radius, and the surface tension are known. The pressure inside the water far away from the bubble can be set equal to the atmospheric pressure (101.325 kPa), as the liquid thickness is only a few mm. The microbubble diameter is measured directly from the digital CCD image and the value of the water surface tension is taken from the literature (21). Table 5 shows the pressure inside the microbubble at three possible bubble interior temperatures—room temperature (20°C), 100°C, and 200°C—for four bubble diameters (40 μm, 100 μm, 135 μm, and 175 μm).

Due to its small physical size, it is very difficult to measure the temperature inside the microbubble. However, once the laser beam is blocked, the small size (microns) of the microheater and the fiber probe itself, which is submerged in water, results in the probe tip cooling off very quickly from temperatures at or beyond the boiling points of most liquids (10). For example, a one-dimensional calculation for the thermal diffusion time of a hot object of size "d" immersed in water with a thermal diffusion coefficient δ (1.4×10^{-7}m^{2}s^{-1}) is given by $\tau = d^2/4\delta$; hence, for an object of size $d = 125$ μm, representative of the fiber probe, $\tau = 0.03$ s. It is therefore reasonable to believe that when the bubble reaches it maximum size (after 150 s for the microbubble of Fig. 4), temperature gradients have disappeared and the temperature inside the bubble is equal to the temperature in the liquid close to the bubble membrane, i.e., ~20°C. For ±10°C around 20°C, the relative pressure spread is <0.5% for any microbubble diameter ranging from 10 to 200 μm. Therefore, the appropriate gas pressure at the maximum bubble diameter can be obtained from the first column ($T = 20$°C) in Table 5; for example, the pressure is ~103 kPa for the bubble diameter of 175 μm.

In addition, the air concentration in the liquid can be calculated. Indeed, using the ideal gas equation, it is easy to show that the air density inside the bubble at its maximum diameter is equal to P_BM/AT_B, where P_B and T_B are, respectively, the pressure and the temperature inside the bubble, M is the molecular mass of the gas contained in the bubble ($M = 0.029$ kg/mol for air), and $A = 8.314$ J/mol K is the gas constant. For the microbubble of Fig. 2 ($D_0 = 95$ μm) at 20°C, its interior pressure is ~104 kPa and the calculated air density is 1.238 kg/m^3. Then, using Eq. 9, the initial air concentration in the liquid has been calculated to be $c_i = 0.022$ kg/m^3 using $\tau_0 = 11$ min (see Fig. 3) and, from Porter et al. (22), $\kappa = 2.42 \times 10^{-9}$ m^2/s and $c_s = 0.023$ kg/m^3.

TABLE 5 Pressure inside microbubbles for various maximum bubble diameters

D (μm)	P_B (Pa) for 20°C	P_B(Pa) for 100°C	P_B(Pa) for 200°C
40	108,600	107,216	105,094
100	104,235	103,681	102,833
135	103,481	103,070	102,442
175	102,988	102,672	102,186

We thank Dr. Geoff Mealing and Dr. Robert Monette from the Institute for Biological Sciences at NRC for providing us with micropipettes and the microinjector. We also acknowledge Dr. Nuch Tanphaichitr, scientific director of the human In Vitro Fertilization Program, Ottawa Health Research Institute for providing us with swine sperm for the trapping experiments and for discussions on sperm-trapping applications. Our thanks also go to our National Research Council (NRC) colleague Dr. Cyril Hnatovsky for introducing Dr. Diop to the microbubble creation technique. We also thank Dr. Linda Johnston at the NRC-Steacie Institute for Molecular Sciences and Dr. Michele Loewen from the NRC-Plant Biotechnology Institute for helpful discussions on cells and for supplying us with the HEK-293 cells, as well as very helpful discussions with Dr. Jana Jass from the Department of Microbiology and Immunology, The University *of* Western Ontario.

This work was funded in part by a Natural Science and Engineering Research Council NanoInnovations grant and a Canadian Institute for Photonic Innovations grant.

REFERENCES

1. Ashkin, A., J. M. Dziedzic, and T. Yamane. 1987. Optical trapping and manipulation of single cells using infrared laser beams. *Nature*. 330: 769–771.
2. Ashkin, A., K. Schütze, J. M. Dziedzic, U. Euteneuer, and M. Schliwa. 1990. Force generation of organelle transport measured in vivo by an infrared laser trap. *Nature*. 348:346–348.
3. Ashkin, A. 1997. Optical trapping and manipulation of neutral particles using lasers. *Proc. Natl. Acad. Sci. USA*. 94:4853–4860.
4. Meiners, J.-C., and S. R. Quake. 2000. Femtonewton force spectroscopy of single extended DNA molecules. *Phys. Rev. Lett.* 84:5014–5017.
5. Chiu, D. T., A. Hsiao, A. Gaggar, R. A. Garza-Lopez, O. Orwar, and R. N. Zare. 1997. Injection of ultrasmall samples and single molecules into tapered capillaries. *Anal. Chem.* 69:1801–1807.
6. Wong, P. K., U. Ulmanella, and C.-M. Ho. 2004. Fabrication process of microsurgical tools for single-cell trapping and intracytoplasmic injection. *J. of Microelectromech. Syst.* 13:940–946.
7. Sato, S., and H. Inaba. 1996. Optical trapping and manipulation of microscopic particles and biological cells by laser beams. *Opt. Quantum Electron.* 28:1–16.
8. Peeters, E. A. G., C. W. J. Oomens, C. V. C. Bouten, D. L. Bader, and F. P. T. Baaijens. 2005. Mechanical and failure properties of single attached cells under compression. *J. Biomech.* 38:1685–1693.
9. Taylor, R. S., and C. Hnatovsky. 2003. Particle trapping in 3-D using a single fiber probe with an annular light distribution. *Opt. Express*. 11:2775–2782.
10. Taylor, R. S., and C. Hnatovsky. 2004. Trapping and mixing of particles in water using a microbubble attached to an NSOM fiber probe. *Opt. Express*. 12:916–928.
11. Lo, C.-M., H.-B. Wang, M. Dembo, and Y.-L. Wang. 2000. Cell movement is guided by the rigidity of the substrate. *Biophys. J.* 79:144–152.
12. Epstein, P. S., and M. S. Plesset. 1950. On the stability of gas bubbles in liquid-gas solutions. *J. Chem. Phys.* 18:1505–1509.
13. Taylor, R. S., and C. Hnatovsky. 2004. Growth and decay dynamics of a stable microbubble produced at the end of a near-field scanning optical microscopy fiber probe. *J. Appl. Phys.* 95:8444–8449.
14. Tanphaichitr, N., J. Smith, S. Mongkolsirikieart, C. Gradil, and C. A. Lingwood. 1993. Role of a gamete-specific sulfoglycolipid immobilizing protein on mouse sperm–egg binding. *Dev. Biol.* 156:164–175.
15. Ambardekar, A. A., and Y.-Q. Li. 2005. Pulsed optical tweezers for levitation and manipulation of stuck biological particles. Proc. Conf. Lasers Electro-optics, Baltimore, USA, May 23rd-27th.
16. Burgos, P., Z. Lu, A. Ianoul, C. Hnatovsky, M.-L. Viriot, L. J. Johnston, and R. S. Taylor. 2003. Near-field scanning optical

microscopy probes: a comparison of pulled and double-etched bent NSOM probes for fluorescence imaging of biological samples. *J. Microsc.* 211:37–47.

17. Ianoul, A., M. Street, D. Grant, J. Pezacki, R. S. Taylor, and L. J. Johnston. 2004. Near-field scanning fluorescence microscopy study of ion channel clusters in cardiac myocyte membranes. *Biophys. J.* 87: 3525–3535.
18. Russell, E. T., M. Lindau, and W. W. Webb. 2001. Robust, high-resolution, whole cell patch-clamp capacitance measurements using square wave stimulation. *Biophys. J.* 81:937–948.
19. Clark, R. S., and A. G. Ewing. 1998. Characterization of electrochemical responses in picoliter volumes. *Anal. Chem.* 70:1119–1125.
20. Brennen, C. E. 1995. Cavitation and bubble dynamics. http://caltechbook.library.caltech.edu/1/00/bubble.htm.
21. Pellicer, J., V. García-Morales, L. Guanter, M. J. Hernández, and M. Dolz. 2002. On the experimental values of the water surface tension used in some textbooks. *Am. J. Phys.* 70:705–709.
22. Porter, T. M., L. A. Crum, P. S. Stayton, and A. S. Hoffman. 2004. Effect of polymer surface activity on cavitation nuclei stability against dissolution. *J. Acoust. Soc. Am.* 116:721–728.